

Coupling between protein-laden films and a shearing bulk flow

A.N. Azadani^a, J.M. Lopez^b, A.H. Hirsaa^{c,*}

^a Department of Mechanical, Aerospace and Nuclear Engineering, Rensselaer Polytechnic Institute, Troy, NY 12180, USA

^b Department of Mathematics and Statistics, Arizona State University, Tempe, AZ 85287, USA

^c Department of Mechanical, Aerospace and Nuclear Engineering, and Department of Chemical and Biological Engineering, Rensselaer Polytechnic Institute, Troy, NY 12180, USA

Received 6 November 2007; accepted 22 February 2008

Available online 6 March 2008

Abstract

Two-dimensional protein crystallization on lipid monolayers at a quiescent air/water interface is now a well-established process, but it only operates under a very restricted set of conditions and on a very slow time scale. We have recently been able to significantly extend the conditions under which the proteins will crystallize as well as speed up the process by subjecting the interface to a shearing flow. Here, we investigate the two-way coupling between a protein-laden film and the bulk flow that provides the interfacial shear. This flow in a stationary open cylinder is driven by the constant rotation of the floor. Using the Boussinesq–Scriven surface model for a Newtonian interface coupled to the Navier–Stokes equations for the bulk flow, we find that the surface shear viscosity of protein-laden films under most conditions is small or negligible. This is the case for films subjected to constant shearing flow, regardless of the duration of the flow. However, when the film is intermittently sheared, significant surface shear viscosity is evident. In these cases, the surface shear viscosity is not uniform across the film.

© 2008 Elsevier Inc. All rights reserved.

Keywords: Surface shear viscosity; Two-dimensional protein crystallization

1. Introduction

The study of protein transport processes in the presence of bulk flow is an emerging field. Many of the studies are focused on quantifying the transport kinetics of proteins in the bulk (liquid) or between the liquid and the gas/liquid interface [1]. These are motivated by diverse applications, ranging from replacement lung surfactant therapy [2] to food sciences, e.g. for making stable emulsions [1].

One of the underlying motivations for the current investigation is to explore the use of fluid dynamics to further our understanding of protein structure, which in turn can advance biological sciences. Further, knowledge of protein structure is the basis for the rational design of new drugs and pharmacological agents. The primary method for determining protein structure and their interaction with ligands is X-ray crystallography.

However, before this powerful technique can be utilized, the protein must first be crystallized. Crystallographers acknowledge that growing crystals is often the major bottleneck in structure determination [3], and fluid dynamics has the potential to improve the situation.

The principle behind protein crystallization is that a protein solution must by some means be transformed to a super-saturated state whereby its return to equilibrium forces exclusion of protein from the solution and into a solid phase, i.e. the crystal. If the super-saturation is too small, the nucleation rate will be so slow that crystals do not form in a reasonable amount of time. On the other hand, if the super-saturation is too large, the probability of spontaneous and uncontrolled nucleation is enhanced which results in extensive and uncontrolled showers of crystals [4]. By virtue of their numbers, none of these crystals grow adequately and they are not suitable for structure studies. Therefore, active control of the conditions, for example, by reducing super-saturation once nucleation has occurred, has been a goal for crystallographers to obtain larger and better-ordered crystals.

* Corresponding author. Fax: +1 518 276 2623.

E-mail addresses: nejata@rpi.edu (A.N. Azadani), lopez@math.asu.edu (J.M. Lopez), hirsaa@rpi.edu (A.H. Hirsaa).

The current interest in 2D protein crystallization stems from the fact that in contrast to growing 3D protein crystals in the bulk, 2D protein crystallization simplifies both the theoretical and experimental aspects of protein studies. For example, 2D systems are not affected by gravity, an issue that plagues 3D crystallographers. Attempts to alleviate this include growing crystals in micro-gravity environments [5]. Another advantage of 2D crystallization is that the protein is concentrated at the interface, requiring much smaller quantities of protein. In practice, this may be crucial for the class of proteins known as membrane proteins due to the difficulty in obtaining large quantities of them. Even for water-soluble proteins, which are of current interest, the relatively high cost of the protein strongly favors 2D crystallization.

The most commonly used approach for 2D crystallization entails the specific binding of a protein to a ligand-embedded monolayer. In practice, dissolved protein is slowly injected into a quiescent aqueous pool on which a ligand-embedded lipid monolayer is initially spread. The protein crystallized most extensively is the bacterial protein streptavidin which is a well-characterized protein and has a high binding affinity to biotin (vitamin-B₇) [6–8]. Several studies have found that streptavidin can be crystallized on a biotinylated lipid monolayer [9–14]. The dissolved streptavidin in the bulk liquid binds to the ligands formed by the biotinylated lipid monolayer initially spread on the liquid surface. Due to a high concentration of protein at the interface and fluidity of the monolayer, the protein self-assembles into the crystal form.

In [15], it was observed that a shearing bulk flow can induce 2D crystallization under conditions where crystallization would not occur in the absence of flow. Here we address how such an evolving surface film, essentially a protein embedded membrane, interacts with the bulk hydrodynamics. Through detailed comparisons between velocity measurements of the protein (crystals and clusters) at the interface and numerical solution of the Navier–Stokes equations coupled to a Newtonian interface (Boussinesq–Scriven surface model), we show that the surface model is applicable over a wide range of conditions.

The flow system utilized is one which we have used previously to study the hydrodynamic coupling between Langmuir monolayers and swirling shear flows with inertia [17,18]. To maximize the signal-to-noise ratio, the experiments were performed at nearly the highest Reynolds number for which the macroscale bulk flow remains axisymmetric. Although high Re flow is not typical of biological systems with protein embedded films, the observed macroscopic response of the protein embedded film to shear (e.g., as expressed by the surface shear viscosity μ^s) is expected to be the same as long as the film remains Newtonian. The flow geometry, namely a stationary cylinder with a free surface, driven by the constant rotation of the floor, is shown in Fig. 1. This flow geometry was selected, in part, because it allows easy optical access to a relatively large portion of the air/water interface. Also, the circular interface with large area-to-perimeter ratio is particularly advantageous in experiments as it minimizes any meniscus effects.

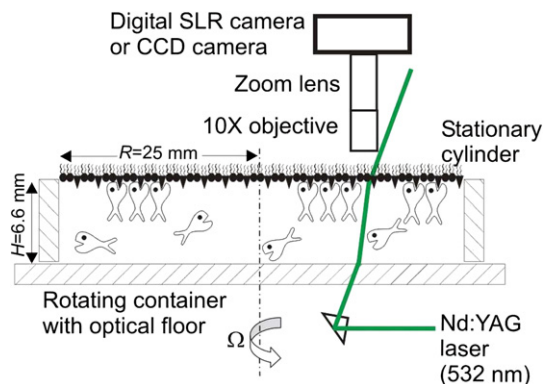


Fig. 1. Schematic of the experimental set-up. The protein crystals (and/or clusters) are illuminated by forward scattering of a laser. The schematic representations of the protein as fish, the ligand as triangles, and diluting lipid as circles, were borrowed from [16].

2. Experimental procedure

The experiments were conducted using the same flow apparatus described in [19]. Aside from its basic features, here we will describe the modifications made to the apparatus for experiments with protein. The flow apparatus consists of a stationary cylinder, made of precision bore glass, with a diameter of $2R = 5.0$ cm and height $H = 0.66$ cm. The cylinder was held by a piece of precision machined Delrin. The Delrin aligned the cylinder axis to within 0.004 cm of the floor axis of rotation. The gap between the bottom of the stationary cylinder and the rotating floor was kept less than 0.008 cm. The rotating floor consisted of an optical quality glass window and made true to within 0.002 cm. Not shown in Fig. 1 is a glass cylinder with larger height and diameter than the stationary cylinder which was bonded to the rotating optical floor in order to form a water-tight rotating container. Thus, there was no need for a seal between the stationary cylinder and the rotating floor.

The use of the Delrin holder for the stationary cylinder along with all the remaining pieces which were made of glass, allowed for thorough cleaning of the surfaces that came in contact with the fluid system between each experiment. Prior to each experiment, the flow apparatus was washed using RBS detergent (PIERCE, catalog no. 27959) to remove any residual protein, then rinsed at least fifteen times with Milli-Q filtered de-ionized water (Millipore Inc.). After the system was allowed to fully dry, high-purity solvent cleaning was performed with acetone. The solvent cleaning procedure was then repeated with methanol, and Milli-Q filtered water. The cleaning prior to each experiment and the use of high-purity materials for the experiment, including water, salt, monolayer forming materials, etc., ensured minimal contamination of the experiment.

For the preparation of the buffer and the monolayer mixture, the procedures in [12,14,20] were followed with some modifications. The experiments were conducted using an aqueous buffer prepared with de-ionized water (Milli-Q filtered, with resistivity greater than 18 M Ω cm). Salt (NaCl, >99.999%, Sigma-Aldrich, catalog no. 204439) was added to make a solution with concentration of 500 milli-molar (mM). Subsequently, sodium phosphate monobasic (NaH₂PO₄, Reagent Plus grade,

>99.0%, Sigma-Aldrich, catalog no. S0751) was added to a concentration of 50 mM. The pH of this buffer was then measured with a pH-meter (Fisher Scientific, Accumet AB15) and found to be 4.34 ± 0.01 . Once the buffer solution was made, it was then filtered to remove any particulates (PES medium, vacuum filter with a pore size of 0.22 μm , Millipore) and stored in a clean container and used within 2 h. The buffer solution was routinely tested to confirm that it was essentially free of surface-active agents (surfactants). In order to verify that the buffer solution was surfactant free, rapid compressions were performed in a Langmuir trough [21]. The surface of the solution was compressed rapidly (in less than 60 s) by an area ratio of 10:1. A decrease in surface tension of less than 0.1 dyn/cm (approximately the resolution of the Wilhelmy balance utilized and of the order of 0.1% of the surface tension of the buffer, 73.69 dyn/cm, which is about 1.39 dyn/cm greater than pure water at the same temperature, due to the presence of the salt) was deemed acceptable. This criteria was also used in earlier studies [21,22], which were sensitive to surface elasticity caused by surfactant contaminants. In the present study, contaminants can interfere with the protein crystallization process. Note that the density, ρ , of a buffer with 500 mM NaCl is $\approx 1.033 \text{ g/cm}^3$, slightly over 3% larger than that of pure water [23]. The dynamic viscosity of such a buffer is $\mu = 0.995 \text{ g/(cm s)}$, or about 4% larger than that of pure water [24].

The monolayer-forming material spread on the free surface consisted of a binary mixture of a biotinylated lipid, which contains the ligand (biotin) onto which the protein (streptavidin) binds, along with a diluting lipid. The purpose of the diluting lipid is to provide an optimal (average) spacing for the ligand molecules and the given protein. The biotinylated lipid used in this study was biotin-X-DHPE (Biotium, catalog no. 60023). Biotin-X-DHPE, in powder form was dissolved in HPLC-grade chloroform and stored at -20°C . The diluting lipid for this experiment was DOPC (Avanti Polar Lipids, catalog no. 850375p), which was dissolved at a concentration of 25 mg/ml and stored under argon at -20°C . Prior to each experiment, the biotin-X-DHPE and DOPC were mixed in a 1:14 molar ratio (0.015 and 0.15 mg/ml, respectively) in a 1:1 mixture of chloroform (Sigma, catalog no. 650498) and hexane (Aldrich, catalog no. 139386) and used within 20 min. The binary mixture was gradually spread (over 3 min) on the surface of the buffer using a 10 μl glass syringe and subsequently allowed to equilibrate for 20 min.

The protein streptavidin, which has a very high binding affinity to biotin, was used in the study. For the present experiments, streptavidin in lyophilized powder form was obtained from *Streptomyces avidinii* (salt free, Sigma, catalog no. S4762). It should be noted that not all batches of the protein would crystallize. Inability to crystallize, probably due to protein inactivity, was not unique to this supplier. Prior to use, the protein was reconstituted in de-ionized water to a concentration of 1 mg/ml prior to storage in a refrigerator. The reconstituted protein was used within 7 days. For each experiment, the protein solution was injected very slowly into the bulk to a concentration of 10 $\mu\text{g/ml}$ after the monolayer had been formed

and allowed to equilibrate. Structural details of streptavidin and the crystals it forms on the interface with a substrate buffer of pH 4.3 are given in [25]. The amount of biotin-X-DHPE molecules at the interface is proportional to the number of streptavidin molecules bound to the lipid monolayer and regulate the surface coverage of the protein molecules at the interface. Specifically, there are $4.1 \times 10^{-8} \text{ g-mol/m}^2$ of streptavidin for each mg/m^2 of the binary lipid mixture. Note that streptavidin has four sub-units, two of which are available for binding to each biotin molecule, and the ratio stated above assumes that all available binding sites are used.

The velocity measurements were performed at the air/water interface, essentially the horizontal plane (r, θ, H), where the azimuthal and radial velocity components were determined. Unlike our previous measurements of interfacial hydrodynamics [21,26], conventional (digital) particle image velocimetry could not be utilized here because the seeding particles would interfere with protein crystallization. Instead, a particle tracking technique was employed using microscopically-imaged solidified protein (crystals/clusters) at the interface as the tracking particles. A CCD camera (Texas Instruments, model 1134P) was used for imaging and the video signal was digitized to a rectangular window by a frame grabber. A window size of 256×192 pixels ($0.9306 \times 0.6096 \text{ mm}$) in the radial and azimuthal directions, respectively, was used. In order to capture the entire air/water interface (50 mm diameter), which is two orders of magnitude larger than the microscopic field of view, the optical system (laser and microscope) was sequentially traversed in the radial direction from the edge of the cylinder to the center over thirty segments with a small overlap. At each radial position, a sufficient number of images was taken in order to capture all of the particles over the given azimuth. Illumination was supplied by a dual oscillator Nd:YAG laser (New Wave Research SOLO I-15 Hz) and the laser oscillators were synchronized using a digital delay/pulse generator (Stanford Research System, model DG535). A time interval of 8 ms between laser pulses was used to provide sufficient particle displacement and to ensure that the majority of the particles remain in a given image pair. The azimuthal and radial velocity components were subsequently determined. Each point on the velocity plots corresponds to an average computed from 25 to 50 particles.

3. Theoretical considerations and numerical computations

The flow is modeled by the axisymmetric Navier–Stokes equations together with the continuity equation and appropriate boundary and initial conditions. Using a cylindrical polar coordinate system (r, θ, z), the Stokes streamfunction, ψ , the axial angular momentum, $\alpha = rv$, and the azimuthal component of vorticity, η , the nondimensional velocity and vorticity vectors are

$$\mathbf{u} = (u, v, w) = \left(-\frac{1}{r} \frac{\partial \psi}{\partial z}, \frac{\alpha}{r}, \frac{1}{r} \frac{\partial \psi}{\partial r} \right),$$

$$\nabla \times \mathbf{u} = \left(-\frac{1}{r} \frac{\partial \alpha}{\partial z}, \eta, \frac{1}{r} \frac{\partial \alpha}{\partial r} \right).$$

The use of ψ and α is convenient in axisymmetric swirling flows; contours of ψ in an (r, z) -plane depict the streamlines in that plane, and contours of α depict the vortex lines.

We use R as the length scale and $1/\Omega$ as the time scale, and define a Reynolds number $\text{Re} = \Omega R^2 \rho / \mu$ to nondimensionalize the axisymmetric Navier–Stokes equations:

$$\frac{D\alpha}{Dt} = \frac{1}{\text{Re}} \nabla_*^2 \alpha, \quad (1)$$

$$\frac{D\eta}{Dt} + \frac{\eta}{r^2} \frac{\partial \psi}{\partial z} - \frac{1}{r^3} \frac{\partial \alpha^2}{\partial z} = \frac{1}{\text{Re}} \left(\nabla^2 \eta - \frac{\eta}{r^2} \right), \quad (2)$$

where

$$\begin{aligned} \nabla_*^2 \psi &= -r\eta, \\ \frac{D}{Dt} &= \frac{\partial}{\partial t} - \frac{1}{r} \frac{\partial \psi}{\partial z} \frac{\partial}{\partial r} + \frac{1}{r} \frac{\partial \psi}{\partial r} \frac{\partial}{\partial z}, \\ \nabla^2 &= \frac{\partial^2}{\partial z^2} + \frac{\partial^2}{\partial r^2} + \frac{1}{r} \frac{\partial}{\partial r}, \\ \nabla_*^2 &= \frac{\partial^2}{\partial z^2} + \frac{\partial^2}{\partial r^2} - \frac{1}{r} \frac{\partial}{\partial r}. \end{aligned} \quad (3)$$

The boundary conditions on the solid boundaries are no-slip, i.e. the normal and tangential derivatives of ψ vanish; $\alpha = 0$ on the stationary cylinder wall and $\alpha = r^2$ on the rotating bottom. The azimuthal vorticity η on the solid boundaries is determined by evaluating (3) on the boundaries once ψ is known. On the air/water interface, being a material surface, ψ is continuous with its value on the sidewalls, which we set to zero without loss of generality. We shall assume that the interface is flat, and hence the contact angle at the air/water/solid contact line is 90° (in the experiment, we fix the location of the contact line by coating the top rim of the glass cylinder with a nonwetting film; also, the Froude number $\text{Fr} = \Omega^2 R^2 / g H \sim 10^{-2}$ for $\text{Re} = 10^3$ used in the experiments). This leaves the conditions for α and η on the interface to be specified.

In our previous studies of this system [21,27] we treated the interface following [28], except that we allowed the surface viscosities to vary with the surfactant concentration. For a flat interface, only the tangential stress balance plays a dynamic role. The tangential stress balance in the azimuthal direction is

$$\frac{\partial v}{\partial z} = \hat{\mu}^s \left(\frac{\partial^2 v}{\partial r^2} + \frac{1}{r} \frac{\partial v}{\partial r} - \frac{v}{r^2} \right) + \frac{\partial \hat{\mu}^s}{\partial r} \left(\frac{\partial v}{\partial r} - \frac{v}{r} \right), \quad (4)$$

and in the radial direction

$$\begin{aligned} \eta &= \frac{1}{\text{Ca}} \frac{\partial \sigma}{\partial r} + (\hat{\mu}^s + \hat{\kappa}^s) \left(\frac{1}{r^2} \frac{\partial^2 \psi}{\partial r \partial z} - \frac{1}{r} \frac{\partial^3 \psi}{\partial r^2 \partial z} \right) \\ &\quad - \frac{1}{r} \frac{\partial^2 \psi}{\partial r \partial z} \frac{\partial (\hat{\mu}^s + \hat{\kappa}^s)}{\partial r} + \frac{2}{r^2} \frac{\partial \psi}{\partial z} \frac{\partial \hat{\mu}^s}{\partial r}, \end{aligned} \quad (5)$$

where $\text{Ca} = \mu \Omega R / \sigma_0$ is the capillary number, $\hat{\mu}^s = \mu^s / \mu R$ is the nondimensional surface shear viscosity and $\hat{\kappa}^s = \kappa^s / \mu R$ is the nondimensional surface dilatational viscosity.

We have found that when the surface has an adequate amount of surfactant ($\gtrsim 0.9 \text{ mg/m}^2$ for the present monolayer, as shown in [15]), the radial component of velocity on the interface is zero, and the interfacial condition in the radial direction reduces

to no-slip, regardless of the physicochemical details of the system [21,27]. Thus, (5) can be replaced by

$$\eta = -\frac{1}{r} \frac{\partial^2 \psi}{\partial z^2}. \quad (6)$$

With the interface suitably covered by the monolayer and the radial surface velocity zero, there is no need to solve an advection-diffusion equation for monolayer concentration. Now the only interfacial parameter in the system is the surface shear viscosity.

The numerical solution of (1)–(3), together with the boundary and interface conditions (4) and (6), follows the method used in [22]. Specifically, the governing equations are discretized in space using second-order center differences and temporal integration is via an explicit second-order predictor-corrector scheme which allows for a straight-forward implementation of the no-slip condition on the solid boundaries and the interfacial stress balances at the air/water interface. In the cylinder of aspect ratio $H/R = 0.264$, 301 grid points were used in the radial and 81 in the vertical directions; these were sufficient to resolve all boundary layers at $\text{Re} = 10^3$. The time-step used was $\delta t = 10^{-4}$. The time to reach steady state is about 100 (corresponding to about 60 s in dimensional time). Further details of the numerical method are omitted as they are available elsewhere [27,29].

4. Results and discussion

It was recently demonstrated that a shearing bulk flow can induce two-dimensional protein crystallization at conditions where crystallization would not occur in the absence of flow [15]. Under quiescent conditions, crystals were found to grow at the interface when the lipid mixture surface concentration exceeded 1.5 mg/m^2 , which corresponds to a surface pressure of 10 dyn/cm , consistent with the observations of others [30]. Below this critical concentration, no crystals were obtained at the interface and only a few bright spots appear where clusters of the protein molecules attach to the ligand sites. However by turning on the flow, protein crystallization was induced at lipid mixture concentrations significantly below the threshold for crystallization in the absence of flow. We were able to obtain crystals at surface pressures of 1.0 and 7.5 dyn/cm , corresponding to 1.0 and 1.39 mg/m^2 lipid mixture concentrations, respectively. Micrographs of crystals and clusters are presented in Fig. 2. Note that the “wide needle” shape of the crystals and their scale (width of order $100 \mu\text{m}$) match exactly those found at this pH (about 4.3) in quiescent systems by others [12,31]. The crystalline nature of the protein is clearly characterized by the sharp and jagged edges evident in Figs. 2a and 2c. The investigation in [15] showed that the interface remains completely covered by the film, that film compression is negligible, and that the only remaining rheological effect of the flow at the interface is due to azimuthal shearing of the film.

In order to investigate the hydrodynamic coupling between the protein-laden film and the bulk hydrodynamics, detailed velocity measurements are performed at the air/water interface. Fig. 3 shows the azimuthal velocity at the interface for the

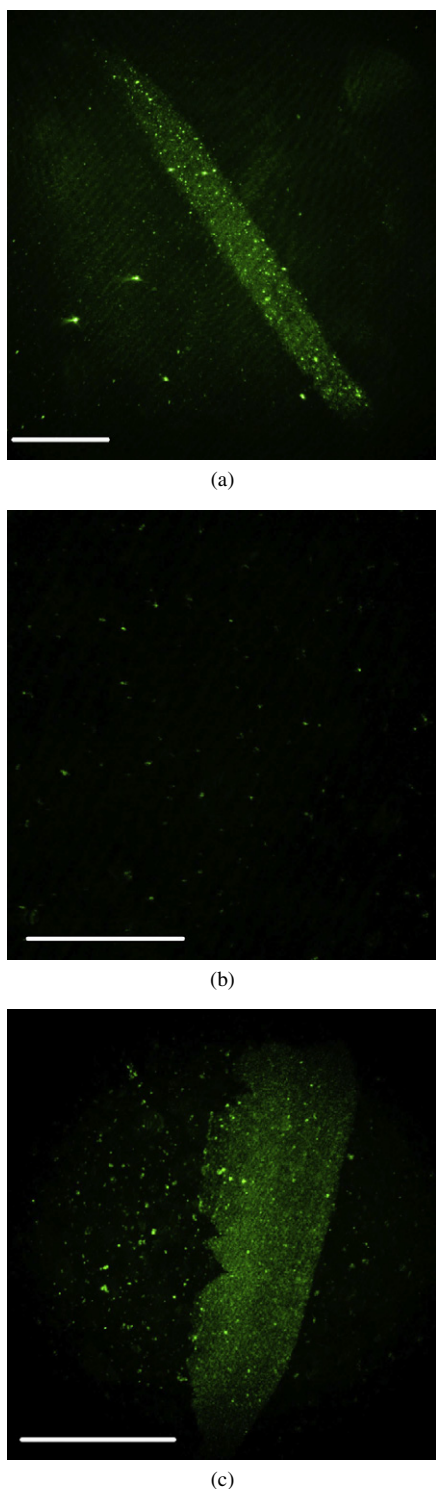


Fig. 2. Micrographs of the air/water interface showing two-dimensional protein crystallization with and without flow. Under quiescent condition, crystallization occurs for a monolayer surface pressure above 10 dyn/cm. The micrograph in (a) is for a quiescent system with surface pressure of 13 dyn/cm corresponding to a surface concentration of 1.68 mg/m². Below the critical surface pressure in the quiescent condition, only clusters of streptavidin attached to the biotinylated lipid monolayer are observed. (b) shows a micrograph at a surface pressure of less than 1.0 dyn/cm corresponding to a surface concentration of 1.0 mg/m² for a quiescent system, where no crystals were found, as expected. (c) shows flow-induced crystals at the same condition as (b), demonstrating that the threshold for protein crystallization is significantly reduced by this flow with $Re = 10^3$. The scale bar for each image is 250 μ m.

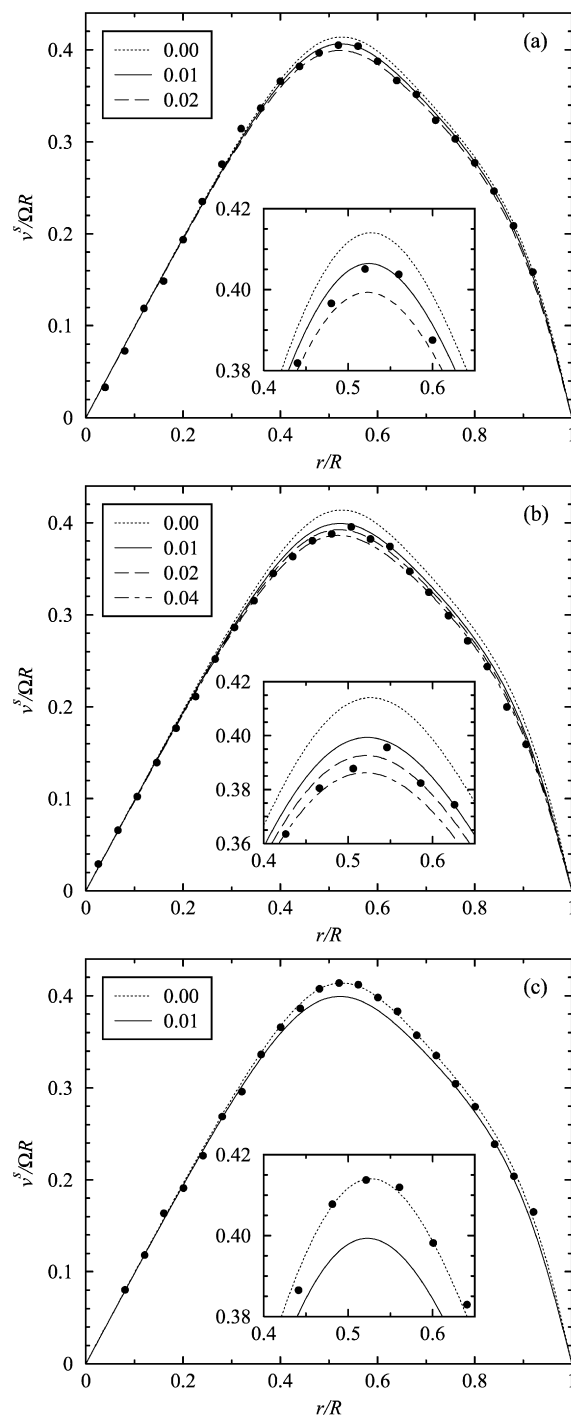


Fig. 3. Experimental (symbols) and computed (lines) azimuthal velocity profiles at the interface for lipid mixture concentrations (a) $C_0 = 1.0$ mg/m², (b) $C_0 = 1.39$ mg/m², and (c) $C_0 = 1.68$ mg/m². The radially stagnant model with uniform λ^s was used, with values as indicated in each panel. In the experiments, the film was subjected to flow for 1 h, where the time sequence of events was: at $t = 0$ protein was injected, at $t = 4$ h flow started, at $t = 4.33$ h velocity measurements began, and at $t = 5$ h measurement ended.

three lipid mixture concentrations studied here (1.0, 1.39, and 1.68 mg/m²), each subjected to flow for one hour. It is important to note that 2D protein crystallization only occurs spontaneously (under quiescent conditions) in the 1.68 mg/m² case. In all the experiments presented here, the flow was started 4 h

after the protein was injected into the bulk. The flow system reaches steady state within about one viscous time unit H^2/ν (about 10 floor rotations, less than 1 min) following a rapid ramp-up from rest [19]. The velocity was measured twenty minutes after the start of the flow, and the measurements took approximately 30 min.

The flow field was computed using a radially stagnant monolayer model [22,27], using (4) and (6) as interfacial conditions, at various values of surface shear viscosity $\hat{\mu}^s$. The comparisons between the measured and computed azimuthal velocity show that the protein-laden film exhibits very small surface shear viscosity, $\hat{\mu}^s \approx 0.01$ (Fig. 3a), $\hat{\mu}^s \approx 0.03$ (Fig. 3b), and $\hat{\mu}^s \approx 0$ (Fig. 3c), at various monolayer concentrations. The general agreement between the experiments and the computed profiles with constant $\hat{\mu}^s$ values demonstrates that the protein-laden monolayer on the buffer solution behaves as a Newtonian interface. The uncertainty in the velocity measurements is of the order of 1% of the maximum velocity or about the size of the symbols used in the plots.

In these cases, the interfacial velocity measurements showed that there is no perceptible radial component of velocity at the interface. Specifically, the measured radial velocity was less than 2.5% of the maximum azimuthal velocity, which is of the order of the uncertainty in the experimental technique utilized. The absence of radial velocity at the air/water interface in the experiment is consistent with the computational results provided in [15], which showed that above a monolayer concentration of about 0.9 mg/m², the secondary flow is unable to reduce the monolayer concentration to zero anywhere on the surface; this forms the basis of the radially-stagnant film model utilized in the present paper.

Experiments with proteins are generally difficult to reproduce, especially those attempting crystallization. In order to confirm the repeatability of the experimental results, velocity measurements were conducted on different days for a particular crystallization condition, and the results agreed to well within experimental uncertainty of 1% [33]. Furthermore, it is difficult to determine protein crystal area coverage in part due to the ambiguity in distinguishing between clusters and crystals, but more importantly due to the difficulty in scanning the interface of a large, flowing system with a microscope. We estimate the area coverage in cases where crystals are observed to be about 10%, however the signal is of the order of the variance of the measurement. In a quiescent system at large supersaturation, [32] gives the area fraction to be as high as 20% for a buffer with pH 4.3. At the shear rates used in our experiment, no deformations of the crystals were detected, and during the short time they are in the field of view of the microscope no rotation can be detected.

The effect of the shearing process was investigated for the 1.68 mg/m² case by subjecting the protein-laden film to different durations of flow. This monolayer concentration was chosen since in this case protein super-saturation is adequate to spontaneously form 2D crystals in the absence of flow. In one case, the film was subjected to flow for three hours (about three times as long as we had subjected the film to flow in the earlier case shown in Fig. 3c), and the resulting velocity profile is shown

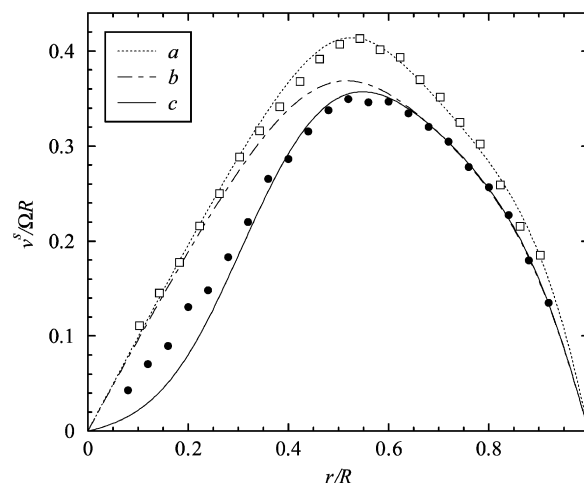


Fig. 4. Azimuthal velocity profiles at the interface for experiments (symbols) with $C_0 = 1.68$ mg/m², and computed profiles using (a) an inviscid monolayer, (b) a viscous monolayer with constant $\hat{\mu}^s = 0.07$, and (c) a viscous monolayer with $\hat{\mu}^s(r) = 0.13[1.05 - \tanh(6r)]$. In the experiments, for the case with the open squares the film was subjected to flow for 3 h (protein was injected at $t = 0$, at $t = 4$ h flow started, at $t = 6.5$ h velocity measurements begun, and at $t = 7$ h measurement ended). The case corresponding to the filled circles the film was subjected to intermittent flow for a total of 2 h (protein was injected at $t = 0$, at $t = 4$ h flow started, at $t = 5$ h flow stopped, at $t = 6.5$ h flow restarted, at $t = 7$ h velocity measurements begun and at $t = 7.5$ h measurements ended).

as open squares in Fig. 4. It is apparent that with continuous shearing this film does not exhibit a significant surface shear viscosity. This was unexpected since 2D crystallization occurs spontaneously without flow in this film, and one would expect such a film to exhibit long-range interactions which would be manifested by a surface (excess) viscosity. It appears that continuous shearing of the film prevents long-range forces from developing. To further investigate this, we used a protocol where the film was sheared with flow for a period of time, then the flow was stopped and the crystals were allowed to grow for an “incubation” period. Subsequently, flow was restarted and the response of the film to shear was measured. The resulting velocity profile is shown as filled circles in Fig. 4. The figure clearly shows that the intermittently sheared film exhibits a significant amount of surface viscosity.

The shape of the velocity profile for the intermittently sheared film is fundamentally different from the continuously sheared cases, where a constant value of $\hat{\mu}^s$ fit the data throughout the air/water interface. Also presented in Fig. 4 are computed profiles corresponding to various interfacial conditions. An inviscid monolayer, of concentration large enough to arrest any radial flow, is shown as case (a). Note that this is the same profile as the $\hat{\mu}^s = 0$ profiles in Fig. 3. A viscous case with a constant value of $\hat{\mu}^s = 0.07$ is shown as case (b). A non-uniform distribution of $\hat{\mu}^s(r) = 0.13[1.05 - \tanh(6r)]$ is presented as case (c). This truncated tanh function has its maximum value of viscosity occurring at the axis and the minimum at the cylinder radius $r = R$. This *ad hoc* distribution was selected to model the crystal-embedded film which is being strongly sheared near the cylinder wall and much less so near the axis. We hypothesize that the crystals formed during

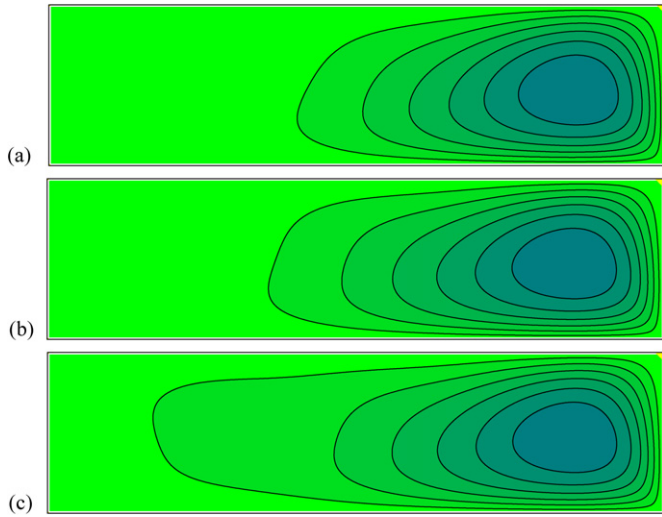


Fig. 5. Computed streamlines (iso-contours of ψ) at $Re = 10^3$ and $H/R = 0.264$. The boundary conditions at the top in cases (a)–(c) are those used in cases (a)–(c) shown in Fig. 4.

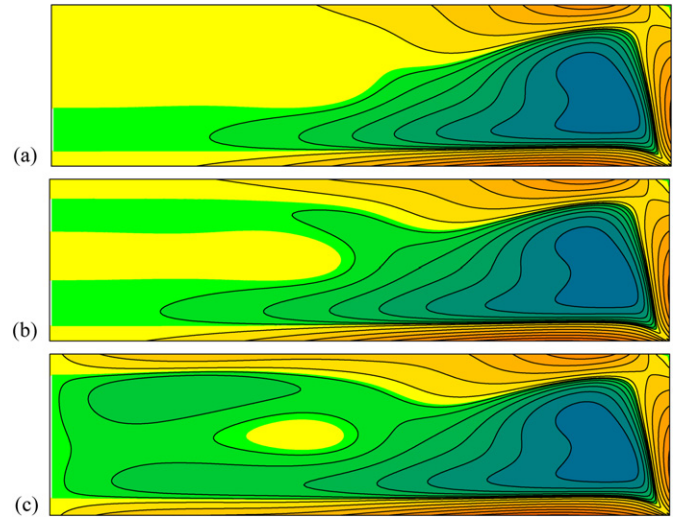


Fig. 7. Computed contours of the azimuthal vorticity η at $Re = 10^3$ and $H/R = 0.264$. The boundary conditions at the top in cases (a)–(c) are those used in cases (a)–(c) shown in Fig. 4.

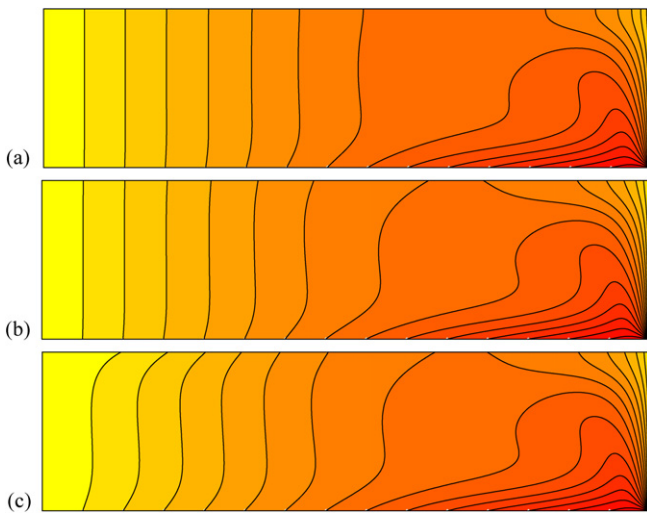


Fig. 6. Computed vortex lines (iso-contours of α) at $Re = 10^3$ and $H/R = 0.264$. The boundary conditions at the top in cases (a)–(c) are those used in cases (a)–(c) shown in Fig. 4.

the incubation protocol can remain more rigid (viscous) near the axis which is more weakly sheared than in the outer part of the interface which is strongly sheared. Although the computed velocity profile using this non-uniform distribution of $\hat{\mu}^s$ does not match the experiment profile very well near the axis, it matches both the value and radial location of the peak velocity and the profile over 70% of the radius. The important point to note is that there is no single constant value of $\hat{\mu}^s$ that can give as good a match for the velocity.

The effects of the various interfacial conditions used to obtain the surface velocity profiles shown in Fig. 4 on the bulk flow are presented in Figs. 5, 6 and 7, showing the streamlines ψ , the angular momentum $\alpha = rv$ (vortex lines) and azimuthal vorticity η . In these plots, the bottom boundary is the rotating floor ($z = 0$), the right boundary is the cylin-

der wall ($r = R$), the left boundary is the axis ($r = 0$), and the top is the air/water interface ($z = H$). The cases (a)–(c) shown in these figures correspond to the same cases presented in Fig. 4.

The inviscid-monolayer covered interface (case a) has the vortex lines normal to the interface, and for $r \lesssim 0.4R$ the bulk flow is essentially in solid-body rotation with the floor (note that the contour levels are quadratically spaced, concentrating more contour levels near zero) with virtually no secondary flow (i.e., the streamfunction is essentially constant for $r \lesssim 0.4R$). All of the secondary overturning circulation is concentrated in the outer radial portion where a well-established boundary layer under the film is evident in the azimuthal vorticity contours. For $r \gtrsim 0.5R$, the vortex lines are bent into the boundary layer on the rotating floor and η is much more intense in this part of the boundary layer. The vortex line bending drives a secondary flow which corresponds to the fluid in the boundary layer being centrifuged radially outward until it meets the stationary cylinder wall and is turned upwards. The structure of the side-wall layer, whose thickness increases linearly with z , is clearly seen in the η -contours. The flow near the interface is radially inward until it reaches the region of solid-body rotation where it is turned back towards the floor boundary layer. The presence of the monolayer immobilizes the interface in the radial direction, leading to $\eta \neq 0$, but the azimuthal velocity at the interface is essentially unaffected by the presence of the inviscid monolayer.

Introducing some surface shear viscosity uniformly across the interface (case b) causes the vortex lines to meet the interface at an angle which depends on both $\hat{\mu}^s$ and the shear at the interface. The resultant vortex line bending reinforces the secondary meridional flow, as illustrated by the streamlines, which now extends to smaller r . The non-uniform $\hat{\mu}^s$ distribution (case c) has a significant impact on the coupling between the interfacial and bulk flows. The immediate difference in the bulk flow is that the vortex lines

are bent much more, particularly for $r \lesssim 0.5R$. This extends the meridional overturning flow further in toward the axis and slows the azimuthal flow at small r on the interface. The resultant azimuthal velocity profile at the interface using this interfacial stress balance gives the best agreement with the measured interfacial velocity profile, as shown in Fig. 4.

5. Concluding remarks

In this paper we described the two-way coupling between a protein-laden film on the air/water interface and a shearing bulk flow. For this shearing flow and the range of monolayer concentrations investigated, the surface tension gradients are adequate to arrest the radial velocity at the interface that is driven by the secondary flow in the bulk; this was confirmed directly by velocity measurements performed on protein crystals or clusters at the interface. In the azimuthal direction, comparisons between measured and computed velocity show that the protein-laden films under most conditions behave as a Newtonian interface which is either inviscid or at most exhibits a small surface shear viscosity. When the protein-laden interfacial film is subjected to intermittent shear, there is evidence that the surface shear viscosity is large and non-uniformly distributed across the film. The macroscale interfacial velocity in such cases can be modeled using a Newtonian interface model with a non-uniform surface shear viscosity distribution, where the shear viscosity is larger in regions where the relatively large and more rigid protein crystals tend to accumulate (primarily toward the axis of rotation, slowly driven by the weak radially inward secondary flow).

We have seen that shearing flow can cause 2D crystallization for systems with lower surface pressure (small supersaturation). We conjecture that in systems with large supersaturation, continuous azimuthal shear prevents the growth of crystals with long-range interactions in the radial direction. Further, by allowing a quiescent period of incubation, such long-range interactions are manifested. When μ^s is being determined in the present experiment, the large shear rate at the interface for $r \gtrsim 0.5R$ has a significant influence on the film itself. This suggests that these films are susceptible to shear-thinning. A systematic study of film response over a wide range of Re needs to be undertaken to shed light on this important issue.

Finally, it is noteworthy that for this investigation of the coupling between a protein-laden interfacial film and the bulk flow, a good description of the resultant interfacial velocity field has been obtained using a fairly standard macroscale Newtonian interface model, albeit with variable surface shear viscosity, to provide a macroscale description of molecular scale processes.

Acknowledgments

This work was partially supported by National Science Foundation grants CTS0340736, CTS0340768, and DMS-0509594.

References

- [1] D. Möbius, R. Miller (Eds.), *Proteins at Liquid Interfaces*, Elsevier, Amsterdam, 1998.
- [2] C. Alonso, A. Waring, J.A. Zasadzinski, *Biophys. J.* 89 (2005) 266.
- [3] A.J. McPherson, *Struct. Biol.* 142 (2003) 1.
- [4] N. Asherie, *Methods* 34 (2004) 266.
- [5] M. Riès-Kautt, I. Broutin, A. Ducruix, W. Shepard, R. Kahn, N. Chayen, D. Blow, K. Paal, W. Littke, B. Lorber, A. Thöbald-Dietrich, R. Giege, *J. Cryst. Growth* 181 (1997) 79.
- [6] L. Chalet, F.J. Wolf, *Arch. Biochem. Biophys.* 106 (1964) 1.
- [7] N.M. Green, *Methods Enzymol.* 184 (1990) 51.
- [8] E.A. Bayer, H. Ben-Hur, M. Wilcheck, *Methods Enzymol.* 184 (1990) 217.
- [9] A.A. Darst, M. Ahlers, P.H. Meller, E.W. Kubalek, R. Blankenburg, H.O. Ribi, H. Ringsdorf, R.D. Kornberg, *Biophys. J.* 59 (1991) 387.
- [10] S.A. Hemming, A. Bochkarev, S.A. Darst, R.D. Kornberg, P. Ala, D.S.C. Yang, A.M. Edwards, *Mol. Biol.* 246 (1995) 308.
- [11] W. Frey, W.R. Schief, V. Vogel, *Langmuir* 12 (1996) 1312.
- [12] S.-W. Wang, C.R. Robertson, A.P. Gast, *J. Phys. Chem. B* 103 (1999) 7751.
- [13] T.C. Edwards, N. Malmstadt, S. Koppenol, H. Masahiko, V. Vogel, P.S. Stayton, *Langmuir* 18 (2002) 7447.
- [14] P. Ratanabanangkoon, A.P. Gast, *Langmuir* 19 (2003) 1794.
- [15] A.N. Azadani, J.M. Lopez, A.H. Hirsra, *Langmuir* 23 (2007) 5227.
- [16] A. Brisson, W. Bergsma-Schutter, F. Oling, O. Lambert, I. Reviakine, *J. Cryst. Growth* 196 (1999) 456.
- [17] R. Miraghaie, J.M. Lopez, A.H. Hirsra, *Phys. Fluids* 15 (2003) L45.
- [18] M.J. Vogel, A.H. Hirsra, R. Miraghaie, J.M. Lopez, *Langmuir* 20 (2004) 5651.
- [19] J.M. Lopez, F. Marques, A.H. Hirsra, R.J. Miraghaie, *J. Fluid Mech.* 502 (2004) 99.
- [20] M.T. Yacilla, C.R. Robertson, A.P. Gast, *Langmuir* 14 (1998) 497.
- [21] A.H. Hirsra, J.M. Lopez, R. Miraghaie, *J. Fluid Mech.* 443 (2001) 271.
- [22] A.H. Hirsra, J.M. Lopez, R. Miraghaie, *J. Fluid Mech.* 470 (2002) 135.
- [23] R.C. Weast, M.J. Astle (Eds.), *CRC Handbook of Chemistry and Physics*, 62nd ed., CRC Press, Boca Raton, FL, 1982.
- [24] J. Kestin, H.E. Khalifa, R.J. Correia, *J. Phys. Chem. Ref. Data* 10 (1981) 71.
- [25] S.-W. Wang, C.L. Poglitsch, M.T. Yacilla, C.R. Robertson, A.P. Gast, *Langmuir* 13 (1997) 5794.
- [26] M.J. Vogel, A.H. Hirsra, J.S. Kelley, G.M. Korenowski, *Rev. Sci. Instrum.* 72 (2001) 1502.
- [27] J.M. Lopez, A. Hirsra, *J. Colloid Interface Sci.* 229 (2000) 575.
- [28] L.E. Scriven, *Chem. Eng. Sci.* 12 (1960) 98.
- [29] J.M. Lopez, A.H. Hirsra, *J. Colloid Interface Sci.* 206 (1998) 231.
- [30] P. Ratanabanangkoon, *Investigating streptavidin crystallization on lipid monolayers and bilayer vesicles*, PhD thesis, Stanford University, 2002.
- [31] P. Ratanabanangkoon, M. Gropper, R. Merkel, E. Sackmann, A.P. Gast, *Langmuir* 18 (2002) 4270.
- [32] M.T. Yacilla, *Influence of pH on two-dimensional crystals of streptavidin*, PhD thesis, Stanford University, 1998.
- [33] A.N. Azadani, *Flow enhanced protein crystallization at the air/water interface*, PhD thesis, Rensselaer Polytechnic Institute, 2007.